Rotational Speed Measurement through Digital Imaging and Image Processing

Yunfan Wang[a], Lijuan Wang[a,b], Yong Yan[a]
[a] School of Engineering and Digital Arts
University of Kent, Canterbury, Kent CT2 7NT, U.K.
[b] School of Control and Computer Engineering
North China Electric Power University, Beijing 102206, China

Abstract—This paper presents a rotational speed measurement system based on a low-cost imaging device with a simple marker on the rotor. Structural similarity and two-dimensional correlation algorithms are deployed to process the images. The measurement principle, structure design and performance assessment of the proposed system are presented and discussed. The effects of different markers, image processing algorithms and illumination conditions on the performance of the measurement system are quantified through a series of experimental tests on a laboratory test rig. Experimental results suggest that the system is capable of providing the maximum relative error of ±1% with normalized standard deviation less than 0.8% over a speed range from 0 to 700 RPM (Revolutions Per Minute).

Keywords—rotational speed; measurement; tachometer; image processing; image similarity evaluation;

I. INTRODUCTION

Rotating machineries such as generators, electromotors and centrifuges are widely used in many industries. As one of the crucial parameters for rotating machineries, rotational speed is useful for system condition monitoring, process control and fault diagnosis. Consequently, online continuous monitoring of rotational speed is essential in a range of industries. Rotational speed measurement devices can be categorized into two types according to their sensing principles: contact and noncontact. The contact tachometers normally have a narrow measurement range and may generate wear on the rotor surface over long time. Alternatively, a variety of noncontact tachometers based on optical, electrical, and magnetic induction principles have been developed [1-4]. However, each technique has their individual limitations and cannot adapt to all industrial environments. For instance, the operation of magnetic tachometers requires a magnet to be installed on the rotor and the system performance is susceptible to electromagnetic interferences. Photoelectric tachometers do not perform well under hostile operating conditions [4]. The electrostatic sensors based rotational speed measurement system is little affected by environmental factors, but it is not suitable for very low speed measurement when less electrostatic charge is generated on the rotor surface [6, 7]. High-speed cameras incorporating sophisticated imaging techniques have been applied to vehicle speed detection and large rotation measurement [7-13]. The measurement accuracy is acceptable, but the cost of the high-speed cameras limits the wide applicability of the technique.

This paper presents the latest development in the use of a low-cost camera for rotational speed measurement incorporating image similarity evaluation and frequency detection techniques. Compared to the conventional methods, the low-cost imaging based rotational speed measurement has advantages, including noncontact measurement, simple installation, low maintenance, wide applicability and high system stability. In addition, the proposed system is simple and cost-effective and has fast-response as it uses structural similarity or correlation processing to represent the rotational periodicity. Experimental tests were conducted on a purpose-built test rig over a rotational speed range from 0 to 700 RPM (Revolutions Per Minute). In this paper the effects of different markers, image processing algorithms and illumination conditions on the performance of the measurement system are analyzed and discussed.

II. MEASUREMENT PRINCIPLE AND METHODOLOGY

A. Measurement principle

When a simple mark is stuck on the cross section of a rotor, the rotational speed of the rotor can be measured through detecting the cyclic patterns in the captured images. As shown in Fig. 1, a low-cost imaging device is applied to continuously capture the images of the rotor. In this study, a common low-cost imaging device (Logitech USB HD Pro C920 Webcam; cost £60) is chosen to assess the performance of the proposed measurement system. The imaging device has a maximum frame rate of 30 frames per second (FPS) and supports USB Video Device Class mode. In order to maintain fast response time of the system, the video is saved as 'I420_160x120' format, which has a total of 19,200 pixels in each image frame. Image similarity evaluation algorithms are used to quantify the similarity between the captured original image and the subsequent images. With the continuous processing of the images, the similarity level is determined and reconstructed as a continuous and periodic time-domain signal. The periodicity of the similarity level is in fact equal to the time of the rotor rotating for one complete revolution. Fast Fourier Transform

(FFT) is used to convert the acquired time-domain signal to the frequency domain. The peak with the highest amplitude is corresponding to the rotational frequency, which is then converted into rotational speed in RPM. In this study the image and signal processing work is completed in a host computer. A user-friendly graphical user interface is developed to achieve real time measurement and presentation of the rotational speed.

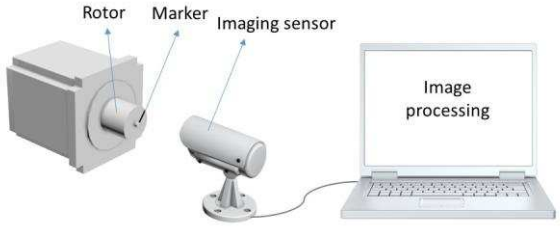

Fig. 1. Structure of the measurement system.

B. Image similarity evaluation

In this study two image processing algorithms, namely, structural similarity (SSIM) and two-dimensional correlation (CORR2) are applied, respectively, to evaluate image similarity in the rotational speed measurement system.

1) SSIM

SSIM [14] is an image quality metric that assesses the visual impact of three aspects of an image: luminance, contrast and structure. It is used for measuring the similarity between two images and designed to improve traditional methods such as peak signal-to-noise ratio and mean squared error, which are inconsistent with human visual perception [10]. SSIM index is a multiplicative combination of three terms l(x,y), c(x,y) and s(x,y) which are corresponding to luminance, contrast and structure between two windows x and y. The local SSIM (x, y) is obtained from:

$$\mathrm{SSIM}(x, y) = [l(x, y)]^{\alpha} \cdot [c(x, y)]^{\beta} \cdot [s(x, y)^{\gamma}] \tag{1}$$

where

$$l(x, y) = \frac{2\mu_x\mu_y + C_1}{\mu_x^2 + \mu_y^2 + C_1} \tag{2}$$

$$c(x, y) = \frac{2\sigma_x\sigma_y + C_2}{\sigma_x^2 + \sigma_y^2 + C_2} \tag{3}$$

$$s(x, y) = \frac{\sigma_{xy} + C_3}{\sigma_x\sigma_y + C_3} \tag{4}$$

where μ_x, μ_y, σ_x, σ_y and σ_{xy} are the local means, standard deviations, and cross-covariance of the two windows x and y, respectively. To simplify the expression (1), set $\alpha = \beta = \gamma = 1$ and $C_3 = C_2/2$. The SSIM index can be described as:

$$\mathrm{SSIM}(x, y) = \frac{(2\mu_x\mu_y + C_1)(2\sigma_{xy} + C_2)}{(\mu_x^2 + \mu_y^2 + C_1)(\sigma_x^2 + \sigma_y^2 + C_2)} \tag{5}$$

The overall structural similarity MSSIM of the two images X and Y is defined as:

$$\mathrm{MSSIM}(X, Y) = \frac{1}{M}\sum_{j=1}^{M} \mathrm{SSIM}(x_j, y_j) \tag{6}$$

where M is the number of local windows in the image and x_j and y_j are the image contents at the j^{th} local window. The larger MSSIM index, the higher similarity between the two images X and Y.

2) CORR2

Correlation is a method for establishing the degree of probability that a linear relationship exists between two measured quantities. Correlation algorithm measures the degree of correlation between the two images with the same size. For two $m \times n$ image matrices X and Y the correlation coefficient r_{ij} is defined as:

$$r_{ij} = \frac{\sum_m \sum_n [X(m+i, n+j) - \bar{X}][Y(m, n) - \bar{Y}]}{\sqrt{\sum_m \sum_n [X(m, n) - \bar{X}]^2 \cdot \sum_m \sum_n [Y(m, n) - \bar{Y}]^2}} \tag{7}$$

where X(m, n) and Y(m, n) are the gray-scale value at the point (m, n) in the images X and Y, respectively. $\bar{X}$ and $\bar{Y}$ are the mean values of the intensity matrices X and Y, respectively. The correlation coefficient has the value r=1 if the two images are absolutely identical, r=0 if there are completely uncorrelated and r=-1 if one of them is an inverted version of the other. As the correlation coefficient is completely invariant to linear transformations of X and Y, it is insensitive to uniform variations in brightness or contrast across an image. However, it is extremely sensitive to the image skewing, pincushioning and vignetting that inevitably occurs in imaging systems [15].

C. Rotational speed calculation

Since the rotor is in rotational motion, the similarity level between the first image and subsequent images is periodic with time. The frequency f of the signal indicating the similarity level is equal to the rotating frequency. Thus the rotational speed n_m in RPM can be calculated from

$$n_m = 60\, f \tag{8}$$

where f can be determined through applying FFT to the reconstructed signal of the similarity level.

III. Experimental Results and Discussion

A. Test rig

As shown in Fig. 2, the measurement system consists of a marker on the cross section of the rotor, the low-cost imaging device to continuously capture videos of the rotor, a laptop to perform the image processing and rotational speed calculation. The rotor is made of Polytetrafluoroethylene (PTFE) with a diameter of 45 mm. The imaging device is connected to the computer and placed immediately opposite to the cross section of the rotor where a marker is seen. Acquired video images are transmitted to the computer via a USB cable for post processing. Rotational speed can be finally calculated in RPM. In order to obtain an independent reference speed to assess the

proposed technique, a contact-type tachometer (Compact Instruments, model A2109) [16] is used in this study. During the experiments the tachometer head was pressed firmly and directly to the rotor end to ensure the instrument is accurately in line with the rotor.

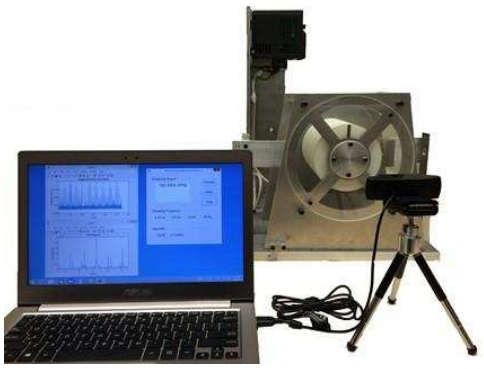

Fig. 2. The integrated rotational speed measurement system.

B. Test program

The test program is summarized in Table I. In order to investigate the effects of marker design on the performance of the measurement system (Test I), different shape, size and position of markers (see Fig. 3) were tested. To create strong colour contrast between the rotor and the marker, the marker is in back colour. In Test II, the effects of the similarity detection algorithms on the measurement results are assessed. Both algorithms are tested under the same experimental conditions. Test III aims to verify the stability of the system under different illumination conditions.

TABLE I. TEST PROGRAM

No.	Test condition						
	Frame-rate (FPS)	Marker			Similarity evaluation	Illumi-nation	n_m (RPM)
		Size (mm)	shape	location			
I	25	5,8,11	strip / circular	centre/ edge/radial	CORR2	Normal (4W)	0-700
II	25	8	strip	radial	SSIM / CORR2	Normal (4W)	0-700
III	25	8	strip	radial	CORR2	Weak (0.8W) / Normal (4W) / Strong (8W)	0-700

(a) Width 5 mm (b) Width 8 mm (c) Width 11 mm

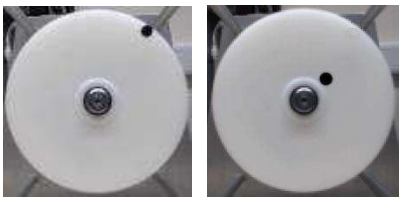

(d) Dimeter 8 mm_Edge (e) Dimeter 8 mm_Centre

Fig. 3. Different markers for the rotational speed measurement.

The flowchart of the rotational speed measurement software is shown in Fig. 4. The measurement commences by starting the video image capture. Consecutive colour images are obtained from the captured images at a constant rate and converted to grayscale for image similarity evaluation using SSIM or CORR2 algorithm. The first frame is compared with the subsequent frames continuously and the results are used to generate a continuous time-domain signal, which contains the periodic pattern in the waveform due to the periodic motion of change over the rotating rotor. FFT is applied to determine the frequency of the rotation. Finally, the rotational speed frequency is converted into RPM.

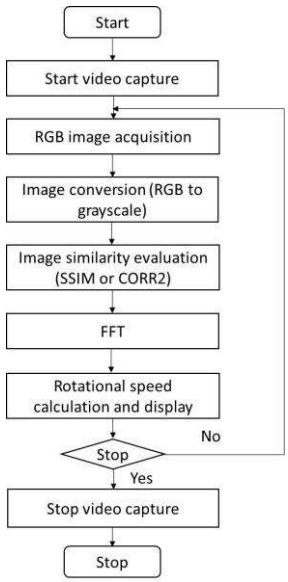

Fig. 4. Flowchart of the measurement software.

C. Effects of marker design

The measurement accuracy is assessed in terms of relative error (e):

$$e = \frac{n_m - n_r}{n_r} \times 100\% \quad (9)$$

where n_m and n_r are the measured and reference speeds. Repeatability is represented in terms of normalized standard deviation of the measured speed, which is defined as:

$$\delta = \frac{\sigma}{\bar{n}_m} \times 100\% \quad (10)$$

where σ and $\bar{n}_m$ are the standard deviation and average value of the measured speed, respectively. It must be pointed out that

the normalized standard deviation of the measured speed includes both the repeatability of the measurement system and fluctuation of the motor rig.

Experimental tests were conducted to explore the effect of maker size and shape on the system performance in terms of accuracy and repeatability. Marker design is an important factor for the proposed system. The shape and colour are not critical issues as long as the marker can be easily recognized from images. Experimental tests were conducted over the rotational speed from 0 to 700 RPM to determine the optimum marker size and position. The CORR2 algorithm was applied for similarity evaluation. Fig. 5 shows the test results when a circular disk with a diameter of 8 mm was placed on the edge and centre of the rotor, respectively, and a strip marker with a width of 8 mm is compared. As expected, the circular disk placed on the edge of the rotor generates more accurate and stable results than that close to the centre, since it travels over a longer angular distance for the same time interval and the difference of the similarity levels is evident. Compared to the circular disk, the strip marker with the same width has a better repeatability as it behaves like an array of multiple disks on the same radius and more information is derived from the images.

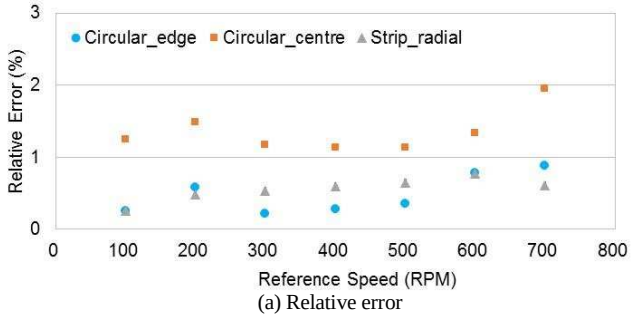

(a) Relative error

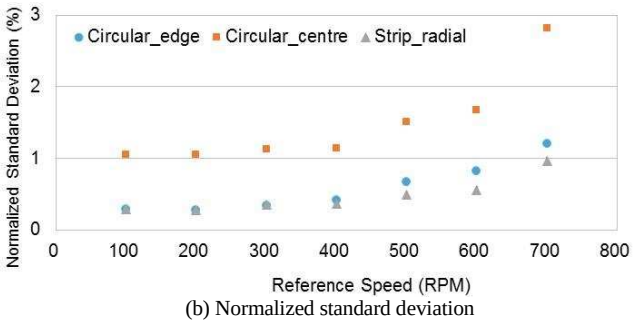

(b) Normalized standard deviation

Fig. 5. Test results for different marker positions.

To further explore the effects of the marker size on the system performance, strip markers with a width of 5 mm, 8 mm and 11 mm were tested, respectively. Results shown in Fig. 6 suggest that the marker with a width of 5 mm yields the best results in terms of accuracy and repeatability. An explanation for this result is that a smaller marker has a better spatial resolution in image analysis and hence produces more accurate and stable results.

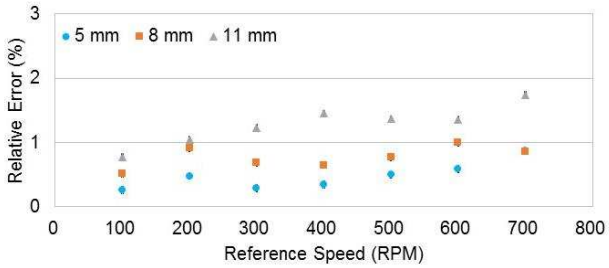

(a) Relative error

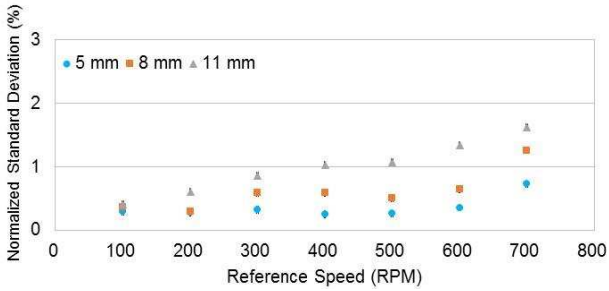

(b) Normalized standard deviation

Fig. 6. Test results for different sized markers.

D. Comparison between SSIM and CORR2

Fig. 7 shows the typical image similarity results obtained under the same test conditions using SSIM and CORR2 algorithms, respectively. We can see that both algorithms yield a similar periodicity of results, but the values of image similarity are different. CORR2 generates a larger similarity index than SSIM as CORR2 only quantifies the pixel intensity of the image. The unexpected spikes in Fig. 7 result from the similarity result between the images, which are believed to be due to the inherent vibration effect of the rotor under relatively high speed. Results in Fig. 8 indicate that CORR2 outperforms SSIM in both accuracy and repeatability at higher speeds (>500 RPM), while both perform similarly at lower speeds (<500 RPM). The reason for this difference is that SSIM considers more visual impacts of the images when computing image similarity, while the CORR2 is insensitive to uniform variations in brightness or contrast across an image. However, either of the methods is suitable for low speed measurement, but not good for high-speed measurement when a fast system response is required and significant vibration is present (which brings interference to the measurement results).

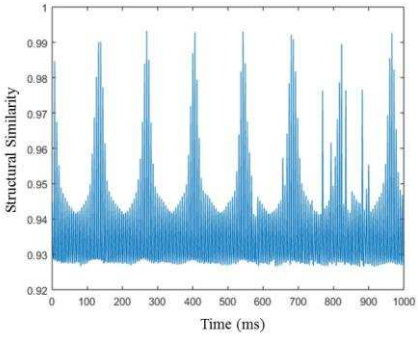

(a) SSIM

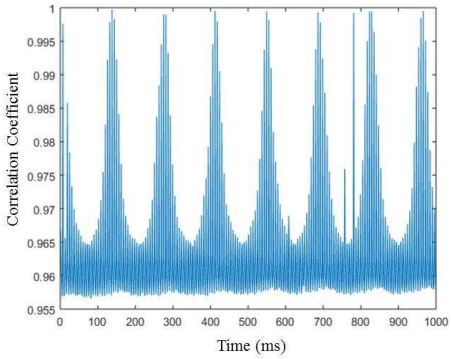

(b) CORR2

Fig. 7. Time domain results for image similarity evaluation.

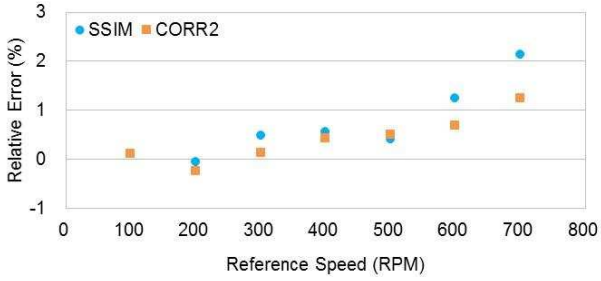

(a) Relative error

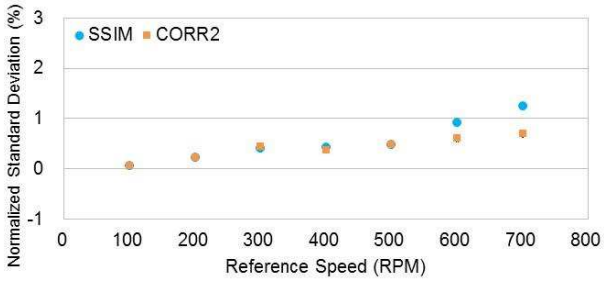

(b) Normalized standard deviation

Fig. 8. Test results for different image processing algorithms.

E. Effects of illumination conditions

Experimental tests were conducted under three different illumination conditions: weak light, normal light and strong light. The three conditions are implemented using a desk lamp with adjustable light intensity: weak (0.8W power), normal (4W power) and strong (8W power). As shown in Fig. 9, the relative error is found almost independent of the illumination conditions, which indicates the robustness of the system under weak or strong illumination conditions. However, the normalized standard deviation under weak and strong illumination conditions is larger than that under normal light, which indicates weak or strong illumination will affect the repeatability of the system. Particularly, the weak light brings the non-uniform contrast between the rotor and the marker and thus increases the uncertainty in image similarity evaluation.

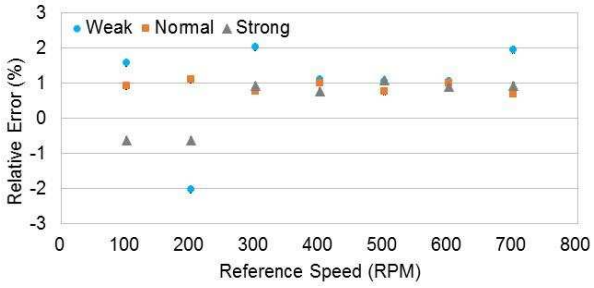

(a) Relative error

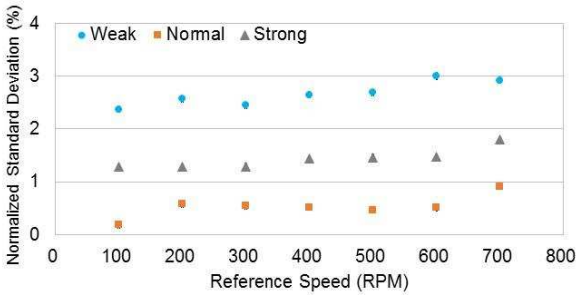

(b) Normalized standard deviation

Fig. 9. Test results under different illumination conditions.

IV. Conculsions

Experimental results under different test conditions suggest that the low-cost imaging device based rotational speed measurement system performs very well in terms of accuracy and repeatability. When the strip marker with a width of 5 mm is applied, the measurement system is capable of providing a relative error of no greater than ±1 % with the maximum normalized standard deviation of 0.8% over the speed range from 0 to 700 RPM. Since these data combine both the repeatability of the speed measurement system and the stability of the test rig, the actual repeatability of the system should be better 0.8%. The image correlation is a more suitable algorithm than SSIM in terms of accuracy and repeatability. It is evident that the system is stable and environmental factors have little effect on the measurement results even under different illumination conditions. However, the current system is limited in a relatively narrow meausremnt range due to the restriction of the frame rate. Future work will focuse on the use of low-cost cameras to achieve higher rotational speed measurement incorporating mathematical modelling techniques.

References

[1] A. Segovia, G. Mayra, L. C. Longoria and A. Diaz, “Stroboscopic microcontroller-based tachometer,” Rev. Sci. Instrum., vol. 70, no. 3, pp. 1875–1879, 1999.

[2] R. Myers, R. A. Islam, M. Karmarkar and S. Priya, “Magnetoelectric laminate composite based tachometer for harsh environment applications,” Appl. Phys. Lett., vol. 91, no. 12, pp. 122904-1–122904-3, 2007.

[3] Y. S. Didosyan, H. Hauser, H. Wolfmayr, J. Nicolics and P. Fulmek, “Magneto-optical rotational speed sensor,” Sens. Actuators A, Phys., vol. 106, nos. 1–3, pp. 168–171, 2003.

[4] Y. Li, F. Gu, G. Harris and A. Ball, “The measurement of instantaneous angular speed,” Mech. Syst. Signal. Pr., vol. 19, pp. 786-805, 2005.

[5] L. Wang, Y. Yan, Y. Hu and X. Qian, “Rotational speed measurement through electrostatic sensing and correlation signal processing,” IEEE Trans. Instrum. Means., vol. 63, no. 5, pp. 1190-1199, 2014.

[6] L. Wang, Y. Yan, Y. Hu and X. Qian, “Rotatioanl spee measurement using single and dual electrostatic sensors,” IEEE Sens. J., vol. 15, no. 3, pp. 1784-1793, 2015.

[7] H. Lin, K. Li and C. Chang, “Vehicle speed detection from a single motion blurred image,” Image Vision Comput., vol. 26, pp. 1327-1337, 2008.

[8] D. Luvizon, B. Nassu and R. Minetto, “A video-based system for vehicle speed measurement in urban roadways,” IEEE Trans. Intell. Transp. Syst., vol. pp, no. 99, pp. 1-12, 2016.

[9] T. Suzuki, H. Nakamura, O. Sadaki amd J. Greivenkamp, “Small-rotation-angle measurement using an imaging method,” Opt. Eng., vol. 40, no. 3, pp. 426-432, 2001.

[10] J. Guo, C. Zhu, S. Lu, D. Zhang and C. Zhang, “Vision-based measurement for rotational speed by improving Lucas-Kanade template Tracking algorithm,” Appl. Optics, vol. 55, no. 25, pp. 7186-7194, 2016.

[11] S. Maji and J. Malik, “Object detection using a Max-Margin Hough Transform,” in Proc. of Computer Vision and Pattern Recognition, pp. 1038-1045, Florida, USA, 20-25 June 2009.

[12] X. Zhu and S. Yu, “Measurement angular velocity based on video technology,” in Proc. of International Congress on Image and Signal Processing (CISP), pp. 1936 – 1940, Shanghai, China,15-17 Oct. 2011.

[13] X. Zhang, J. Chen, Z. Wang, N. Zhan and R. Wang, “Digital image correlation using ring template and quadrilateral element for large rotation measurement,” Opt. Lasers Eng., vol. 50, no. 7, pp. 922–928, 2012.

[14] Z. Wang, A. C. Bovik, H. R. Sheikh and E. P. Simoncelli, “Image quality assessment: From error visibility to structural similarity,” IEEE Transactions on Image Processing, vol. 13, no. 4, pp. 600-612, 2004.

[15] A. Kaur, L. Kaur and S. Gupta, “Image recognition using coefficient of correlation and structural similarity index in uncontrolled environment,” Intel. J. Comput. Appl., vol. 59, no. 5, Dec. 2012.

[16] A2109 Advent Contact / Optical Tachometer, Available online: 378 http://www.compactinstruments.co.uk/shop/advent-range/a2109lsr/ (accessed on 10 October 2016).